



Global and Northern-High-Latitude Terrestrial carbon sinks in the 21st century from CMIP6 experiments

Han Qiu^{1,2*}, Dalei Hao², Yelu Zeng¹, Xuesong Zhang³, Min Chen^{1,4*}

¹Department of Forest and Wildlife Ecology, University of Wisconsin-Madison

5 ²Atmospheric Sciences and Global Change Division, Pacific Northwest National Laboratory, Richland, WA, USA

³USDA-ARS Hydrology and Remote Sensing Laboratory, Beltsville, MD 20705-2350 USA

⁴Center for Climatic Research, Nelson Institute, University of Wisconsin-Madison

Correspondence to: Han Qiu (han.qiu@pnnl.gov) and Min Chen (min.chen@wisc.edu)

Abstract. Climate warming is accelerating the changes in the global terrestrial ecosystems and particularly those in the northern high latitudes (NHL), and rendering the land-atmosphere carbon exchange highly uncertain. The Coupled Model Intercomparison Project Phase 6 (CMIP6) employs the most updated climate models to estimate terrestrial ecosystem carbon dynamics driven by a new set of socioeconomic and climate change pathways. By analyzing the future (2015-2100) carbon fluxes estimated by ten CMIP6 models, we quantitatively evaluated the projected magnitudes, trends and uncertainties of global and NHL carbon fluxes under four scenarios plus the role of NHL in the global terrestrial ecosystem carbon dynamics. Overall, the models suggest that the global and NHL terrestrial ecosystems will be consistent carbon sinks in the future, and the extent of the carbon sinks is projected to be larger under scenarios with higher radiative forcing. By the end of this century, the models by average estimate the NHL net ecosystem productivity (NEP) as 0.54 ± 0.77 , 1.01 ± 0.98 , 0.97 ± 1.62 , and 1.05 ± 1.83 PgC/yr under SSP126, SSP245, SSP370 and SSP585, respectively. The uncertainties are not substantially reduced compared with earlier results, e.g., the Coupled Climate Carbon Cycle Model Intercomparison Project (C4MIP). Although NHL contributes a small fraction of the global carbon sink (~13%), the relative uncertainties of NHL NEP are much larger than the global level. Our results provide insights into future carbon flux evolutions under future scenarios and highlight the urgent need to constrain the large uncertainties associated with model projections for making better climate mitigation strategies.

25



1 Introduction

The global terrestrial biosphere is considered as a major carbon pool and a key player in the global carbon cycle. In the last decade (2011-2020), the terrestrial biosphere absorbs CO₂ from atmosphere at a rate of about 120 Pg C/year by vegetation photosynthesis and releases a similar amount of carbon back to the atmosphere through
30 respirations from plant metabolism and microbial activities (i.e., autotrophic and heterotrophic respirations), resulting in a land carbon sink of about 3.4 Pg C/year (Friedlingstein et al., 2020). However, these numbers change over time in response to climate change and are associated with large uncertainties. For example, using trace gas measurements, Campbell et al., (2017) estimated a large increase in global terrestrial biosphere photosynthetic carbon uptake of 31% over the 20th century accompanied with rapidly rising CO₂ concentration and warming
35 climate. This estimate however did not agree with many carbon/climate models. The global soil respiration carbon flux has also been found increasing in the past several decades, according to the analysis of a global soil respiration database, but the degree to which climate change affects the changes of heterotrophic respiration is highly uncertain (Bond-Lamberty et al., 2018). Besides the scientific importance of understanding the long-term feedbacks between the terrestrial biosphere and the climate system, it is also critical to track the changes of the global land carbon sink
40 for making manageable climate mitigation policies as it is a key component of the global carbon budget and has been considered as an important approach to achieve carbon neutrality.

Particularly, as the host of the most Earth's permafrost soils, arctic ecosystems store twice the amount of carbon as in the atmosphere and play an important role in the global carbon budget (Schuur et al., 2015; Tarnocai et al., 2009; Zimov et al., 2006). During the last 30 years, the temperature in northern high-latitudes (NHL) regions has
45 risen 0.6 °C per decade, almost double the rate of the rest of the world (IPCC, 2013). Previously stored soil carbon is potentially labilized by the thawing of permafrost and enhanced decomposition of soil organic carbon due to a warmer climate (Belshe et al., 2012; Koven et al., 2011; Natali et al., 2014; Schaefer et al., 2011; Schuur et al., 2015; Schuur and Abbott, 2011). This shapes a positive climate feedback since the excessive carbon release would in turn stimulate climate warming (Koven et al., 2011; Schuur & Abbott, 2011; Zimov et al., 2006). On the other
50 hand, CO₂ fertilization combined with other favorable conditions could enrich plant growth and drive the expansion of vegetation, e.g., arctic tundra and boreal forest, in the Arctic region, which may enhance plant carbon uptake and photosynthesis productivity (Berner et al., 2020; Liang et al., 2018; Mekonnen et al., 2019; Myers-Smith et al., 2020; Sistla et al., 2013). Despite the prevailing greening signal observed in the NHL, regional browning or negative



Normalized Difference Vegetation Index (NDVI) trend was also observed (Lara et al., 2018; Phoenix and Bjerke, 55 2016). Disturbances such as fire are also increasing in frequency and duration in response to the warming climate change, and exerting impacts on vegetation dynamics (Hu et al., 2015; Mekonnen et al., 2019; Whitman et al., 2018). These evolving and counteracting processes complicate the determinations whether the NHL ecosystem functions as a carbon source or sink and how this will be projected in the future. Great uncertainties are revealed from evaluating results of multiple Earth system models (ESMs) in the NHL region, with some ESMs showing NHL 60 ecosystems as a carbon sink while others indicating an opposite sign (Fisher et al., 2014; Friedlingstein et al., 2014; Qian et al., 2010). Moreover, inconsistent model structure, diversified process representations as well as uncertainties in data, external variables and parameterizations further compromise the confidence in predictions of ESMs (Bradford et al., 2016; Luo et al., 2016; Todd-Brown et al., 2013).

The Coupled model intercomparison project (CMIP) coordinated a series of comprehensive comparisons among 65 a handful climate models from around the world and has become an essential element of international climate research (Eyring et al., 2016b; Taylor et al., 2012). Building on in the previous Atmospheric Model Intercomparison Project (AMIP) twenty years ago, CMIPs have broadened its purposes and contributions to a wide range of disciplines to foster understanding of evolutions and changes of climate and its impacts on societal sectors from history, to present and future (Eyring et al., 2016b). Yet, great uncertainties were revealed from previous CMIPs' 70 results and the spread of the model responses to climate sensitivity remains large (Collins et al., 2013). A primary scientific gap of previous CMIP experiments is how the radiative forcing pathways, resulting from anthropogenic activities or natural emissions, could be optimally estimated (Stouffer et al., 2017). More recently, the 6th phase CMIP (CMIP6) employed a number of the most updated global climate models and endorsed 21 individually designed MIPs to address various scientific questions (Eyring et al., 2016b). Guided by the goals to facilitate 75 integrated research on the impact of future scenarios over natural and human systems, and to help quantify uncertainties in future projections based on multi-model simulations, the most devoted MIP - the Scenario Model Intercomparison Project (ScenarioMIP; O'Neill et al., 2016) incorporate a broad range of future scenarios with various combinations of Representative Concentration Pathways (RCPs) which was initially adopted in CMIP5 and newer Shared Socioeconomic Pathways (SSPs). These integrations allow a comprehensive assessment of plausible 80 future climate conditions covering a wide span of mitigation and adaptation options (Riahi et al., 2017; van Vuuren et al., 2014), and represent the most updated understanding of the climate change and carbon cycle in the next few



decades (Eyring et al., 2016b; O'Neill et al., 2016). The CMIP6 ScenarioMIP takes advantage of previous CMIP resources and makes advancements in two major updates: first, the climate models employed are more updated with better representations of underlying physical processes; and second, the models are driven by a new set of emission pathways and land use scenarios, i.e., SSPs generated by updated versions of Integrated Assessment Models (IAMs) produced by newly updated data (O'Neill et al., 2016). The variety of SSPs and RCPs combinations also cover a broader range of air pollutant emissions which are supposed to bridge the gap of relatively narrow aerosol scenarios adopted in CMIP5 (Stouffer et al., 2017).

The goal of this study is thus to answer the following questions based on the CMIP6 ScenarioMIP results: a) What is the future trajectory (spatial and temporal patterns) of global and NHL terrestrial carbon sinks? b) What is the relative role of NHL in global terrestrial ecosystem carbon sink? and c) What is the magnitude of the model uncertainties related to the answers to the first two questions?

2 Materials and Methods

This study focuses on investigating the Net Ecosystem Productivity (NEP) at both global and NHL (poleward of 50 °N) scales from existing CMIP6 outputs. For diagnosing purposes, we also analyzed the Net Primary Productivity (NPP) and Heterotrophic Respiration (RH), since they represent the two primary components of NEP: net plant carbon uptake and respirational carbon loss due to microbial decomposition, as $NEP = NPP - RH$. These model outputs were obtained from Earth System Grid Federation (ESGF) (<https://esgf-node.llnl.gov/search/cmip6/>, accessed on Oct. 1st, 2021) which unified the standardization to provide data access to various model outputs (Eyring et al., 2016b, a). Each model in CMIP6 was conducted with an ensemble of simulations with different initial conditions which were categorized and labeled with four variant indices: the realization index (*r*), the initialization index (*i*), the physics index (*p*) and the forcing index (*f*) (Eyring et al., 2016b; Petrie et al., 2020). To uniformly control the model conditions in case of unexpected uncertainties, we confined the selection of model outputs to experiments with all variant indices labeled with 'I', i.e. 'rIiIpIfI', for consistency. In particular, the ScenarioMIP experiments endorsed a set of future global change scenarios, i.e. the combinations of SSPs and RCPs, to represent the alternative evolutions of societal development, emissions and concentrations (O'Neill et al., 2016). The RCPs are a set of four future greenhouse gas emission pathways in which the end-of-century radiative forcing approaches four target levels (2.6, 4.5, 6.0, and 8.5 W/m²), i.e. RCP2.6, RCP4.5, RCP3.7, RCP8.5 (van Vuuren et al., 2011). The four target



forcing levels are set to be realized by altering future greenhouse gas emissions and by changing underlying
110 socioeconomic projections. The SSPs were developed to describe a set of five future global socio-economic
development scenarios (SSP1 to SSP5). Four future scenarios with different SSP and RCP combinations, i.e.
SSP1+RCP2.6 (SSP126), SSP2+RCP4.5 (SSP245), SSP3+RCP7.0 (SSP370), SSP5+RCP 8.5 (SSP585) were
considered in this study to cover a variety of future climate change projections. Overall, nine models with ten
115 datasets were selected in this study, i.e. the ACCESS-ESM1-5 (Ziehn et al., 2020), BCC_CSM2-MR (Wu et al.,
2019), CanESM5 (Swart et al., 2019), NorESM2-LM (Seland et al., 2020), NorESM2-MM (Seland et al., 2020),
CESM2-WACCM (Gettelman et al., 2019; Lawrence et al., 2019), CMCC-CM2-SR5 (Cherchi et al., 2019), EC-
Earth3-Veg (Wyser et al., 2020), IPSL-CM6A-LR (Dufresne et al., 2013), MPI-ESM1-2-LR (Mauritsen et al.,
2019; Reick et al., 2013). The NorESM2-LM and NorESM2-MM share the same horizontal resolution of ocean and
120 atmosphere component. We hereafter abbreviate the nine models with ten datasets as ten models in the rest part of
this article. The detailed information with land and atmosphere components and spatial resolutions, as well as key
relevant model features are listed in Table 1.

We used monthly NEP, NPP, RH, land surface temperature (TS) and atmospheric CO₂ concentration from the
ten CMIP6 models with data availability over the historical period (1980-2014) and under the four future scenarios
125 (2015-2100) in our analyses. We aggregated NEP, NPP and RH from different models and scenarios to global and
NHL scales as the area-weighted sum of all belonging grids, whereas for TS, area-weighted mean was used. The
bottom (i.e., nearest to the land surface) layer atmospheric CO₂ concentration was employed and aggregated into
global and NHL scales. Note that only four out of the ten models have available CO₂ data to date. The calculated
monthly values were further aggregated into the yearly scale for analysis. The annual model outputs with various
130 spatial resolutions were resampled with a consistent grid resolution of 1 degree (mesh size: 320 × 160) for generating
the spatial trend maps. The ensemble model projections and uncertainties of NEP, NPP, RH and TS were evaluated
by calculating the multi-model mean (μ) and standard deviations (SD, σ) of the yearly model outputs at both the
global and NHL scale. Meanwhile, the contribution of model SD relative to the mean is quantified by the coefficient
of variation (CV), $CV = \sigma/\mu$, to interpret the relative magnitude of the model uncertainty. We estimated the temporal
135 trends of μ and SD using linear least square regression method to quantitatively analyze the ensembled model
behavior as a function of time. Meanwhile, the historical annual NEP was evaluated with estimates from the Global



Carbon Project (GCP; Friedlingstein et al., 2020). Additionally, sensitivity analyses for different carbon fluxes to climate drivers were performed by calculating flux changes in response to the temperature rises at an increment of 1°C and atmosphere CO₂ concentration at an increment of 1 ppm for each model at both the global and NHL scales.

140 Finally, we evaluated trends of the NHL carbon fluxes changes relative to the global carbon fluxes changes under the future scenarios. The flux changes were calculated using the future annual carbon fluxes subtract the 2015 carbon flux.

3 Results

3.1 Magnitudes of global and NHL NEP

145 Figure 1 shows the annual NEP in the historical (1980-2014) and future periods (2015-2100) under the four global change scenarios from the ten CMIP6 models. On average, the ten CMIP6 models indicate a strong global terrestrial ecosystem carbon sink (positive NEPs) of 4.48 ± 0.54 Pg C/year (annual mean \pm interannual standard deviation) during the historical period, with a large spread across individual models (Fig S1). As a benchmark, the estimates from the GCP show the global terrestrial ecosystems as a consistent carbon sink during the historical

150 period at 2.43 ± 0.97 Pg C/year, which is lower than the model ensemble mean. The models also estimate positive NHL NEPs as 0.56 ± 0.11 Pg C/year during the historical period.

Over the future years, the CMIP6 models suggest the global terrestrial ecosystems continue as a carbon sink under all four scenarios (5.56 ± 0.88 , 6.69 ± 0.78 , 7.26 ± 0.98 and 8.13 ± 1.56 Pg C/year for SSP126, SSP245, SSP370 and SSP585, respectively according to the mean of the ten models). For NHL, the carbon sink is estimated

155 as 0.79 ± 0.59 , 0.95 ± 0.14 , 0.94 ± 0.16 and 1.01 ± 0.18 Pg C/year for SSP126, SSP245, SSP370 and SSP585, respectively. However, a few models indeed suggest the global terrestrial ecosystems as a carbon source at the end of the 21st century under SSP126, such as CanESM5 and EC-Earth3-Veg. In the NHL, while most models suggest a carbon sink, the model BCC-CSM2-MR estimates a carbon source even though it shows the global ecosystem as a consistent carbon sink, irrespective of the model scenarios.



160 3.2 Trends of global and NHL carbon fluxes in the 21st century

Referencing to the average condition in 2015-2020, the CMIP6 models show the global mean land TS will increase by 1.17, 2.45, 4.03, and 5.22 °C by the end of 21st century (2095-2100) under SSP126, SSP245, SSP370 and SSP585, respectively. The growth of TS in NHL is projected to increase by 2.41, 4.47, 7.14, and 9.41 °C by the end of this century under the four scenarios respectively, which are exclusively higher than the global projections (Figure S2 and Table 2). The atmospheric CO₂ concentrations are projected to increase at similar rates during 2015-2100 at global and NHL scales with 0.52, 2.36, 5.43 and 8.51 ppm/year, under SSP126, SSP245, SSP370 and SSP585, respectively (Figure S5).

In response to the elevating temperature, NPP and RH from the CMIP6 models (Figure S3 and S4) show positive trends under all four scenarios and the trends are larger under the warmer (higher TS) scenarios at both global and NHL scales. Global NPP will increase at rates of 65.72, 196.48, 294.87 and 387.75 Tg C/year² under SSP126, SSP245, SSP370 and SSP 585, respectively. NHL NPP are projected to grow at rates of 16.16, 41.33, 61.06, and 79.32 Tg C/year² accordingly. Except SSP126, similarly positive but generally smaller trends were found for RH at both global and NHL scales (Figure S4, Table 2), thus cancelled a majority part of the NPP growth and resulted in small growing NEPs.

CMIP6 models show a trend of NEP that first increases until the middle of the 21st century and then decreases at both NHL and global scales under SSP126. Overall, they show a slightly decreasing trend at NHL (-2.84 Tg C/year²) and global (-22.50 Tg C/year²) scales during 2015-2100 under SSP126. The trends are positive under SSP245 at 8.93 Tg C/year² at the global scale, and 2.54 Tg C/year² for NHL. Under SSP370 and SSP585, the positive trends become more prominent: they are 20.08 and 44.40 Tg C/year² at the global scale, and 3.08 and 4.27 Tg C/year² in the NHL under SSP370 and SSP585, respectively.



3.3 Divergent carbon flux estimations among the CMIP6 models

180 Large uncertainties of estimated global and NHL NEP were found, measured by the standard deviation (SD) across the CMIP6 models. The average SD for global NEP over the historical period was 2.85 PgC/year, and it expands to 3.96, 4.51, 5.44 and 5.60 Pg C/year by the end of the 21st century under SSP126, SSP245, SSP370 and SSP585, respectively. Specifically, the model uncertainties of global and NHL NEP conserve under SSP126 with small shrinking trends of SD values (-2.84 Tg C/year² and -0.22 Tg C/year² for global and NHL respectively; Table 2). For SSP245, SSP370 and SSP585, 185 the model uncertainties tend to expand towards the end of this century for both global and NHL scales. The model uncertainties are the largest under SSP370 and SSP585. Globally, the mean NEP values for SSP370 and SSP585 are 6.08 Pg C/year and 7.77 Pg C/year, respectively, during the (2095-2100) with concomitant large SDs of 7.84 Pg C/year (CV = 129%) and 8.53 Pg C/year (CV = 109.78%). It is worth noting that the mean NEP values for SSP370 and SSP585 in NHL are 0.77 Pg C/year and 0.84 Pg C/year, respectively, during 2095-2100, while the SDs are relatively huge: 1.64 Pg C/year (CV = 190 213.00%) and 1.86 Pg C/year (CV = 221.43%) accordingly. Similarly, huge uncertainties for NPP and RH were identified. The average SD for global and NHL NPP over the historical period were 14.89 and 1.51 PgC/year, respectively, and they were projected to expand at rates of 50.10, 138.01, 219.68, 284.02 TgC/year (global) and 4.64, 8.87, 18.07 and 26.87 TgC/year (NHL) under SSP126, SSP245, SSP370 and SSP585, respectively. For RH, the global and NHL average SD over the historical period were 16.15 and 1.66 PgC/year, respectively, and they were projected to expand at rates of 18.54, 36.27, 195 55.39, 72.56 TgC/year (global) and 4.06, 7.76, 16.63, and 23.52 TgC/year (NHL) under SSP126, SSP245, SSP370 and SSP585, respectively.

The large uncertainties of NEP are likely due to the uncertainty of CMIP6 estimated NPP and RH in response to the temperature changes and the CO₂ fertilization effects in each model. The uncertainties of TS projections by the end of the 21st century are 2.59, 2.80, 2.60, 2.73 °C in the NHL, which are much larger than the uncertainties of global TS at 0.89, 0.89, 200 0.97, and 1.24 °C, under SSP126, SSP245, SSP370 and SSP585, respectively. As shown in Figure 2, the CMIP6 estimated annual carbon fluxes have strong linear relationships to TS. For NPP, a 1 °C increase of global TS corresponds to an increase of global annual NPP from 0.47 to 13.34 Pg C/year; in the NHL, the range spans from 0.28 to 0.95 Pg C/year. Global annual RH will increase at rates from 1.06 to 11.12 Pg C per 1 °C increase of global TS, and the rates are between 0.28 and 1.29 Pg C/year for the NHL annual RH. All the lowest sensitivities are estimated by ACCESS-ESM-1-5 and the



205 highest sensitivities are from CanESM5. As the residual of NPP and RH, the sensitivities of NEP to TS are more complicated: the global annual NEP will change at a rate between -0.59 (by ACCESS-ESM-1-5) and 2.21 Pg C/year (by CanESM5) per 1 °C increase of global TS; and the changing rates are between -0.37 (by BCC-CSM2-MR) and 0.23 Pg C/year (by CanESM5) for the NHL annual NEP. The linear trend patterns of the three carbon fluxes relative to the CO₂ fertilization are similar with the linear trend patterns relative to the temperature rise for the four models with available data, 210 as shown in Figure 3. The NPP gain at a rate from 0.037 PgC/year per ppm CO₂ concentration rise in model IPSL-CM6A-LR to 0.064 PgC/year in model BCC-CSM2-MR globally, and from 0.008 PgC/year in model MPI-ESM1-2-LR to 0.011 PgC/year in model BCC-CSM2-MR at the NHL scale. The RH gain at a rate from 0.030 PgC/year per ppm CO₂ concentration rise in model IPSL-CM6A-LR to 0.058 PgC/year in model BCC-CSM2-MR globally, and from 0.007 PgC/year in model IPSL-CM6A-LR to 0.015 PgC/year in model BCC-CSM2-MR at the NHL scale. The NEP show 215 contrasting trends at the two different scales relative to the CO₂ concentration rise for model BCC-CSM2-MR: at global scale, NEP is positive correlated with CO₂ concentration rise, while at NHL scale they are negatively correlated. The other three models show slight positive trends of NEP fluxes relative to the CO₂ concentration rise at both scales. There remains a strong linear relationship between TS and atmospheric CO₂ concentrations irrespective of the model scenarios (Figure S6), which could explain the similar trend patterns of carbon fluxes change in response to the TS and CO₂ concentration rise in 220 Figure 2 and Figure 3.

3.4 Latitudinal distributions of NEP

Figure 4 shows NEP in the 10°-latitudinal bins between 60°S and 90°N in the historical, the early (2015-2024), the middle (2050-2059) and the end (2091-2100) decades of the 21st century under the four scenarios. Overall, the global 225 ecosystems were projected as a stronger carbon sink under SSP245, SSP370 and SSP585 than the historical period for most of the latitudes except the polar region (>80 °N) where the NEP remains relatively constant. Under SSP126, there is a drawdown during 2091-2100 between 20 °S to 10 °N. Among all the latitudinal bins, the tropical regions near the equator act as the largest carbon sink with the highest uncertainties. However, the uncertainties at 60 °N and 70 °N are exclusively larger relative to the absolute values of NEP in this region (i.e., the CV values), which are 109.44%, 264.11% under SSP126,



230 86.37%, 173.89% under SSP245, 106.92%, 364.27% under SSP370, and 119.60%, 484.50% under SSP585, comparing with those near the equator of 100.32%, 58.94%, 80.46%, 54.58% for the four future scenarios, accordingly.

3.5 Spatial pattern of trends of NHL carbon fluxes

235 According to the average of CMIP6 model projections, Figure 5 shows significant positive trends of NPP and RH, but mixed trends of NEP in the NHL under all of the four scenarios. With growing radiative forcing or temperature from SSP126 to SSP585, the positive trends of NPP and RH increase everywhere in the NHL. The spatial pattern of NEP trends is more complicated. Under SSP126, most of the forested area in the NHL were projected to have significantly decreasing NEP, while the other regions show no significant trends. More area turns to have significant positive and larger NEP trends with
240 larger radiative forcing levels from SSP126 to SSP245 and SSP370. Under SSP585 which shows the highest level of radiative forcing and global warming, most of the NHL NEP, particularly areas covered by forest, are projected to have significant positive trends, while the tundra area in Northern Canada and Siberia are in contrast have significant negative trends.

3.6. The role of NHL in future global carbon fluxes changes

245 The CMIP6 models show consistent positive contribution of the NHL to the global carbon fluxes changes since 2015, measured by slopes of linear regression models between the NHL and global numbers (Figure 6). On average, the CMIP6 models estimate that NHL contributes 16% of global NPP increase under SSP126 and 20% under the other three scenarios, and contributes 23%-26% of global RH increase under the four scenarios. For NEP, the NHL's contributions are between 7% and 11%. However, it is worth noting that some of these contributions are with high uncertainties from different models.
250 For example, CanESM5 generally projects largest increases of global and NHL NPP and RH, but stands out to suggest the lowest NHL contribution (i.e., the smallest slopes) to global NPP and RH. The uncertainties (measured by the standard deviation of the slopes estimated by the ten models) are relatively lower for NPP and RH and scenarios with lower radiative forcing levels, but become high for NEP under high radiative forcing scenarios. For instance, the uncertainties could be as high as five-fold of the contribution estimated by the multi-model means for NEP under SSP370 and SSP585.



In this analysis, we presented the quantification of the future magnitudes, trends, patterns and uncertainties of terrestrial ecosystem carbon fluxes from an ensemble of ten CMIP6 models, with a particular focus on the Arctic-Boreal regions in the Northern high latitudes. The CMIP6 models estimate the global terrestrial ecosystems as a strong carbon sink but with a magnitude that is 2.06 Pg/year or 85% higher than the estimates from the benchmarking global carbon project, suggesting consideration of bias corrections when using CMIP6 modeled carbon fluxes for other applications, particularly those sensitive to the magnitude of these carbon fluxes.

On average, the CMIP6 models project large increases of NPP and RH in the global and NHL terrestrial ecosystems in the future, while the NHL is projected to grow 1.43, 1.13, 1.31, 1.40 times faster for NPP and 1.47, 1.46, 1.58, 1.55 times faster for RH, under SSP126, SSP245, SSP370 and SSP585, respectively, relative to their historical levels than the global scale (Table 2) because of the combination of larger increase of temperature, CO₂ fertilization effect, and their higher responsiveness to the warming climate (Figure 2). Such concurrent rising NPP and RH was widely evidenced and discussed in previous literature. Jeong et al., (2018) showed that long-term measurements of CO₂ revealed increasing carbon cycling rates and decreasing soil carbon residence time in the Arctic. On one hand, greening of the world was widely identified due to more favorable vegetation growth conditions promoted by a warming climate (Piao et al., 2020; Zhu et al., 2016), and warmer temperature and CO₂ fertilization was revealed to enhance the terrestrial gross primary production in the NHL (Liang et al., 2018; Myers-Smith et al., 2020; Wenzel et al., 2016). On the other hand, the increases in RH in response to temperature rise could be attributed to two major reasons (Bond-Lamberty et al., 2018). One reason for the rising RH could result from more active soil bacteria metabolism, and thus enhanced SOM minimization due to rising temperature (Crowther et al., 2016; Lu et al., 2013). The second reason could be the more abundant availability of substrates for metabolism from accelerated ecosystem carbon uptake and debris production (Bond-Lamberty et al., 2018).

The carbon cycling in terrestrial ecosystems is complex and many past and ongoing ecological studies sought to understand the underlying mechanisms. Long term measurements at FLUXNET sites have evidenced greater bioavailable carbon stock due to the faster increasing gross primary production than the concurrent rises of ecosystem respiration in response to the climate change (Falge et al., 2002). However, contradictory conclusions were drawn in some regions of the world where reduced soil carbon stocks were found due to more carbon efflux than influx (Naidu and Bagchi, 2021). The



case in the NHL is even more special, partly because the biological processes such as the vegetation phenology and soil decomposition are especially sensitive to climate change due to the extremely cold environment and the relatively faster temperature change rates (McGuire et al., 2009; Richardson et al., 2018). The thawing of permafrost is changing the soil water balance and increasing the thickness of the active layer, which renders the ancient carbon under potential decomposition (Belshe et al., 2012; Schuur et al., 2015; Schuur & Abbott, 2011). Moreover, the terrestrial carbon fluxes are influenced by the evolutions of various other climate factors, such as precipitation, soil moisture and atmospheric nitrogen deposition (Naidu and Bagchi, 2021; Sierra et al., 2015; Yue et al., 2017). Ultimately, the carbon balance will be determined by the difference between rising primary productivity and the accelerated soil carbon decomposition driven by the interplay of multiple climate drivers (McKane et al., 1997; Sistla et al., 2013). These complex processes have been reflected in the results of our CMIP6 analysis. As the residual between the carbon influx (NPP) and efflux (RH), global and NHL NEP are projected to have more complicated changing patterns. The global and NHL NEP be growingly positive in the future, but at lower rates than NPP and RH. While global NEP is generally higher under warmer scenarios, NHL NEP is at similar levels by the end of the 21st century under different warming levels (e.g., SSP245, SSP370, SSP585; Figure 1). This is partially due to the varying response of different ecosystems to the warming climate, as forest-dominated area is becoming a larger carbon sink and tundra-dominated area is likely becoming a stronger carbon source (Figure 4).

Yet, it is important to note that there remain large uncertainties of the magnitudes and trends of the carbon balance in the global and NHL terrestrial ecosystems. The underlying carbon cycling processes are difficult to quantify and are poorly constrained in current ESMs (Bradford et al., 2016). Sensitivities of carbon fluxes in ESMs are divergent in responses to different climate change drivers (e.g., Figure 2 and Figure 3), such that model uncertainties are pronounced in various aspects (Bradford et al., 2016). Although different land surface models share the similar carbon fluxes transfer mechanisms among different carbon pools, they are diversified in the pool structures (Shao et al., 2013; Yan et al., 2014) and parameterizations (Luo and Schuur, 2020). The categorizations of plant functiontypes (PFTs) are also different among the 10 ESMs (Table 1), for example, CanESM5 has 9 PFTs while CESM2-WACCM has 15 PFTs plus additional crop types. Most models have the nitrogen cycles coupled with carbon cycles with exceptions of CanESM5 and IPSL-CM6A-LR (Table 1). For compensation, IPSL-CM6A-LR adopts the ‘dowregulation’ function to limite the maximum photosynthesis rates to



account for nutrient limitations (Boucher et al., 2020), while the CanESM5 has no nutrient limitations accounted (Swart et al., 2019). This could be one of the reasons CanESM5 has the largest sensitivities of NPP and RH fluxes in response to the climate change (Figure 2). Comprehensive and standard validations of multiple variables are needed to assess the model performance and uncertainties of biogeochemical simulations across CMIP6 models (Spafford and MacDougall, 2021).

310 In our analysis, the uncertainties of the carbon fluxes across the CMIP6 models tend to increase over time, and they grow faster under warmer scenarios. The NHL NEP has more relative uncertainties as opposed to the mean compared with global NEP, and this difference is more pronounced in scenarios with higher radiative forcing levels. By 2100, the CMIP6 models suggest the NHL as a carbon sink of 0.54 ± 0.77 , 1.01 ± 0.98 , 0.97 ± 1.62 , and 1.05 ± 1.83 Pg C/year under SSP126, SSP245, SSP370 and SSP585, respectively, which are exclusively larger than the previous C4MIP results under IPCC SRES

315 A2 scenario with temperature rise of approximately 3.4 (2.0–5.4) °C by 2100 (0.3 ± 0.3 PgC/ year; Qian et al., 2010). The relative uncertainties (SD/mean) for the four scenarios are 143.59%, 97.03%, 167.01% and 174.29% which are at the similar or larger levels than the C4MIP results (100%), indicating the uncertainty level is not reduced in the new models. Moreover, models show distinct sensitivities of carbon fluxes in response to the future temperature rise. While NPP and RH show uniformly positive response to temperature rise, NEP changes could be either positive or negative for different models. The

320 uncertainties in soil carbon dynamics and various projections of soil carbon stock and changes in different CMIP5 models were broadly evaluated and discussed in previous studies (Friedlingstein et al., 2014; Todd-Brown et al., 2013, 2014; Yan et al., 2014). Recent evaluations of soil carbon stock and sequestration of CMIP6-LUMIP models also showed large differences among different CMIP6 models, which in another way indicates the possible uncertainties of soil carbon dynamics stemming from simulating the land-use impacts in different CMIP6 models (Ito et al., 2020). All the CMIP6

325 model results present in this analysis do predict rising NPP and RH in response to temperature rise in the future but with divergent trends and patterns. Consequently, large uncertain or even irreconcilable NEP results in the NHL is shown among different models.



5 Conclusion

330 The climate model intercomparison project is a major approach to quantify and understand the future terrestrial ecosystem carbon cycle and its interactions with the climate system. In this study, we presented the trends and patterns of future projections of carbon fluxes (particularly the net ecosystem productivity) in the global and Northern-high-latitude ecosystems, from a set of the most up-to-date CMIP6 models. Based on the average of the CMIP6 models, our analysis showed that global and NHL ecosystems were and would continue to be carbon sinks, although large uncertainties were
335 found for the size and trends of the carbon sinks among different CMIP6 models, which are not obviously attenuated compared with previous model intercomparison project results. Although the warming levels and sensitivity of ecosystems to the warming temperature are higher in the NHL, the contribution of NHL to the global NEP increase is small, however with larger relative uncertainties. The model uncertainties are pronounced in the historical simulations and are projected to expand wider in the future under scenarios with larger radiative forcing levels. These results revealed the emergent necessity
340 to make endeavors to bridge the knowledge gaps between process parameterization and representations of various ESMs and the real-world processes, as well as to deepen the understanding of the underlying mechanisms of the feedforward and feedback roles of the NHL ecosystem in response to climate change.

345 Acknowledgments, Samples, and Data

We acknowledge the World Climate Research Programme, which, through its Working Group on Coupled Modelling, coordinated and promoted CMIP6. We thank the climate modeling groups for producing and making available their model output, the Earth System Grid Federation (ESGF) for archiving the data and providing access, and the multiple funding agencies who support CMIP6 and ESGF, as well as the efforts of all involved modeling centers.

350 Data and code availability: The CMIP6 model results are public available at ESGF website: <https://esgf-node.llnl.gov/search/cmip6/>. The codes for processing the data and generating the figures are available at: <https://github.com/qhgogogo/CMIP6-carbonflux>.

Han Qiu, Yelu Zeng and Min Chen are supported by the National Aeronautics and Space Administration (NASA) through Terrestrial Ecology: Arctic Boreal Vulnerability Experiment (ABOVE) grants NNH18ZDA001N (award number 80HQTR19T0055) to Min Chen. This work was supported in part by the U.S. Department of Agriculture, Agricultural
355 Research Service. USDA is an equal opportunity provider and employer.



References

- Belshe, E. F., Schuur, E. a. G., Bolker, B. M., and Bracho, R.: Incorporating spatial heterogeneity created by permafrost thaw into a landscape carbon estimate, 117, <https://doi.org/10.1029/2011JG001836>, 2012.
- 360 Berner, L. T., Massey, R., Jantz, P., Forbes, B. C., Macias-Fauria, M., Myers-Smith, I., Kumpula, T., Gauthier, G., Andreu-Hayles, L., Gaglioti, B. V., Burns, P., Zetterberg, P., D'Arrigo, R., and Goetz, S. J.: Summer warming explains widespread but not uniform greening in the Arctic tundra biome, 11, 4621, <https://doi.org/10.1038/s41467-020-18479-5>, 2020.
- Bond-Lamberty, B., Bailey, V. L., Chen, M., Gough, C. M., and Vargas, R.: Globally rising soil heterotrophic respiration over recent decades, 560, 80–83, <https://doi.org/10.1038/s41586-018-0358-x>, 2018.
- 365 Boucher, O., Servonnat, J., Albright, A. L., Aumont, O., Balkanski, Y., Bastrikov, V., Bekki, S., Bonnet, R., Bony, S., Bopp, L., Braconnot, P., Brockmann, P., Cadule, P., Caubel, A., Cheruy, F., Codron, F., Cozic, A., Cugnet, D., D'Andrea, F., Davini, P., Lavergne, C. de, Denvil, S., Deshayes, J., Devilliers, M., Ducharne, A., Dufresne, J.-L., Dupont, E., Éthé, C., Fairhead, L., Falletti, L., Flavoni, S., Foujols, M.-A., Gardoll, S., Gastineau, G., Ghattas, J., Grandpeix, J.-Y., Guenet, B., Guez, L., E., Guilyardi, E., Guimberteau, M., Hauglustaine, D., Hourdin, F., Idelkadi, A., Joussaume, S., Kageyama, M., 370 Khodri, M., Krinner, G., Lebas, N., Levavasseur, G., Lévy, C., Li, L., Lott, F., Lurton, T., Luysaert, S., Madec, G., Madeleine, J.-B., Maignan, F., Marchand, M., Marti, O., Mellul, L., Meurdesoif, Y., Mignot, J., Musat, I., Ottlé, C., Peylin, P., Planton, Y., Polcher, J., Rio, C., Rochetin, N., Rousset, C., Sepulchre, P., Sima, A., Swingedouw, D., Thiéblemont, R., Traore, A. K., Vancoppenolle, M., Vial, J., Vialard, J., Viovy, N., and Vuichard, N.: Presentation and Evaluation of the IPSL-CM6A-LR Climate Model, 12, e2019MS002010, <https://doi.org/10.1029/2019MS002010>, 2020.
- 375 Bradford, M. A., Wieder, W. R., Bonan, G. B., Fierer, N., Raymond, P. A., and Crowther, T. W.: Managing uncertainty in soil carbon feedbacks to climate change, 6, 751–758, <https://doi.org/10.1038/nclimate3071>, 2016.
- Campbell, J. E., Berry, J. A., Seibt, U., Smith, S. J., Montzka, S. A., Launois, T., Belviso, S., Bopp, L., and Laine, M.: Large historical growth in global terrestrial gross primary production, 544, 84–87, <https://doi.org/10.1038/nature22030>, 2017.
- 380 Cherchi, A., Fogli, P. G., Lovato, T., Peano, D., Iovino, D., Gualdi, S., Masina, S., Scoccimarro, E., Materia, S., Bellucci, A., and Navarra, A.: Global Mean Climate and Main Patterns of Variability in the CMCC-CM2 Coupled Model, 11, 185–209, <https://doi.org/10.1029/2018MS001369>, 2019.
- Collins, M., Knutti, R., Gutowski, W., Brooks, H., Shindell, D., and Webb, R.: Long-term Climate Change: Projections, Commitments and Irreversibility, 2013.
- 385 Crowther, T. W., Todd-Brown, K. E. O., Rowe, C. W., Wieder, W. R., Carey, J. C., Machmuller, M. B., Snoek, B. L., Fang, S., Zhou, G., Allison, S. D., Blair, J. M., Bridgman, S. D., Burton, A. J., Carrillo, Y., Reich, P. B., Clark, J. S., Classen, A. T., Dijkstra, F. A., Elberling, B., Emmett, B. A., Estiarte, M., Frey, S. D., Guo, J., Harte, J., Jiang, L., Johnson, B. R., Kröel-Dulay, G., Larsen, K. S., Laudon, H., Lavallee, J. M., Luo, Y., Lupascu, M., Ma, L. N., Marhan, S., Michelsen, A., Mohan, J., Niu, S., Pendall, E., Peñuelas, J., Pfeifer-Meister, L., Poll, C., Reinsch, S., Reynolds, L. L., Schmidt, I. K., Sistla, S., Sokol, N. W., Templer, P. H., Treseder, K. K., Welker, J. M., and Bradford, M. A.: Quantifying global soil carbon losses in 390 response to warming, 540, 104–108, <https://doi.org/10.1038/nature20150>, 2016.
- Dufresne, J.-L., Foujols, M.-A., Denvil, S., Caubel, A., Marti, O., Aumont, O., Balkanski, Y., Bekki, S., Bellenger, H., Benschila, R., Bony, S., Bopp, L., Braconnot, P., Brockmann, P., Cadule, P., Cheruy, F., Codron, F., Cozic, A., Cugnet, D., de Noblet, N., Duvel, J.-P., Ethé, C., Fairhead, L., Fichet, T., Flavoni, S., Friedlingstein, P., Grandpeix, J.-Y., Guez, L., Guilyardi, E., Hauglustaine, D., Hourdin, F., Idelkadi, A., Ghattas, J., Joussaume, S., Kageyama, M., Krinner, G., 395 Labetoulle, S., Lahellec, A., Lefebvre, M.-P., Lefevre, F., Levy, C., Li, Z. X., Lloyd, J., Lott, F., Madec, G., Mancip, M., Marchand, M., Masson, S., Meurdesoif, Y., Mignot, J., Musat, I., Parouty, S., Polcher, J., Rio, C., Schulz, M., Swingedouw,



- D., Szopa, S., Talandier, C., Terray, P., Viovy, N., and Vuichard, N.: Climate change projections using the IPSL-CM5 Earth System Model: from CMIP3 to CMIP5, *Clim Dyn*, 40, 2123–2165, <https://doi.org/10.1007/s00382-012-1636-1>, 2013.
- 400 Eyring, V., Righi, M., Lauer, A., Evaldsson, M., Wenzel, S., Jones, C., Anav, A., Andrews, O., Cionni, I., Davin, E. L., Deser, C., Ehbrecht, C., Friedlingstein, P., Gleckler, P., Gottschaldt, K.-D., Hagemann, S., Juckes, M., Kindermann, S., Krasting, J., Kunert, D., Levine, R., Loew, A., Mäkelä, J., Martin, G., Mason, E., Phillips, A. S., Read, S., Rio, C., Roehrig, R., Senftleben, D., Sterl, A., van Ulft, L. H., Walton, J., Wang, S., and Williams, K. D.: ESMValTool (v1.0) – a community diagnostic and performance metrics tool for routine evaluation of Earth system models in CMIP, 9, 1747–1802, <https://doi.org/10.5194/gmd-9-1747-2016>, 2016a.
- 405 Eyring, V., Bony, S., Meehl, G. A., Senior, C. A., Stevens, B., Stouffer, R. J., and Taylor, K. E.: Overview of the Coupled Model Intercomparison Project Phase 6 (CMIP6) experimental design and organization, 9, 1937–1958, <https://doi.org/10.5194/gmd-9-1937-2016>, 2016b.
- 410 Falge, E., Baldocchi, D., Tenhunen, J., Aubinet, M., Bakwin, P., Berbigier, P., Bernhofer, C., Burba, G., Clement, R., Davis, K. J., Elbers, J. A., Goldstein, A. H., Grelle, A., Granier, A., Guðmundsson, J., Hollinger, D., Kowalski, A. S., Katul, G., Law, B. E., Malhi, Y., Meyers, T., Monson, R. K., Munger, J. W., Oechel, W., Paw U, K. T., Pilegaard, K., Rannik, Ü., Rebmann, C., Suyker, A., Valentini, R., Wilson, K., and Wofsy, S.: Seasonality of ecosystem respiration and gross primary production as derived from FLUXNET measurements, *Agricultural and Forest Meteorology*, 113, 53–74, [https://doi.org/10.1016/S0168-1923\(02\)00102-8](https://doi.org/10.1016/S0168-1923(02)00102-8), 2002.
- 415 Fisher, J. B., Sikka, M., Oechel, W. C., Huntzinger, D. N., Melton, J. R., Koven, C. D., Ahlström, A., Arain, M. A., Baker, I., Chen, J. M., Ciais, P., Davidson, C., Dietze, M., El-Masri, B., Hayes, D., Huntingford, C., Jain, A. K., Levy, P. E., Lomas, M. R., Poulter, B., Price, D., Sahoo, A. K., Schaefer, K., Tian, H., Tomelleri, E., Verbeeck, H., Viovy, N., Wania, R., Zeng, N., and Miller, C. E.: Carbon cycle uncertainty in the Alaskan Arctic, 11, 4271–4288, <https://doi.org/10.5194/bg-11-4271-2014>, 2014.
- 420 Friedlingstein, P., Meinshausen, M., Arora, V. K., Jones, C. D., Anav, A., Liddicoat, S. K., and Knutti, R.: Uncertainties in CMIP5 Climate Projections due to Carbon Cycle Feedbacks, *J. Climate*, 27, 511–526, <https://doi.org/10.1175/JCLI-D-12-00579.1>, 2014.
- 425 Friedlingstein, P., O’Sullivan, M., Jones, M. W., Andrew, R. M., Hauck, J., Olsen, A., Peters, G. P., Peters, W., Pongratz, J., Sitch, S., Le Quéré, C., Canadell, J. G., Ciais, P., Jackson, R. B., Alin, S., Aragão, L. E. O. C., Arneeth, A., Arora, V., Bates, N. R., Becker, M., Benoit-Cattin, A., Bittig, H. C., Bopp, L., Bultan, S., Chandra, N., Chevallier, F., Chini, L. P., Evans, W., Florentie, L., Forster, P. M., Gasser, T., Gehlen, M., Gilfillan, D., Gkritzalis, T., Gregor, L., Gruber, N., Harris, I., Hartung, K., Haverd, V., Houghton, R. A., Ilyina, T., Jain, A. K., Joetzjer, E., Kadono, K., Kato, E., Kitidis, V., Korsbakken, J. I., Landschützer, P., Lefèvre, N., Lenton, A., Lienert, S., Liu, Z., Lombardozzi, D., Marland, G., Metzl, N., Munro, D. R., Nabel, J. E. M. S., Nakaoka, S.-I., Niwa, Y., O’Brien, K., Ono, T., Palmer, P. I., Pierrot, D., Poulter, B., Resplandy, L., Robertson, E., Rödenbeck, C., Schwinger, J., Séférian, R., Skjelvan, I., Smith, A. J. P., Sutton, A. J., Tanhua, T., Tans, P. P.,
- 430 Tian, H., Tilbrook, B., van der Werf, G., Vuichard, N., Walker, A. P., Wanninkhof, R., Watson, A. J., Willis, D., Wiltshire, A. J., Yuan, W., Yue, X., and Zaehle, S.: Global Carbon Budget 2020, 12, 3269–3340, <https://doi.org/10.5194/essd-12-3269-2020>, 2020.
- 435 Gettelman, A., Mills, M. J., Kinnison, D. E., Garcia, R. R., Smith, A. K., Marsh, D. R., Tilmes, S., Vitt, F., Bardeen, C. G., McInerney, J., Liu, H.-L., Solomon, S. C., Polvani, L. M., Emmons, L. K., Lamarque, J.-F., Richter, J. H., Glanville, A. S., Bacmeister, J. T., Phillips, A. S., Neale, R. B., Simpson, I. R., DuVivier, A. K., Hodzic, A., and Randel, W. J.: The Whole Atmosphere Community Climate Model Version 6 (WACCM6), 124, 12380–12403, <https://doi.org/10.1029/2019JD030943>, 2019.



Hu, F. S., Higuera, P. E., Duffy, P., Chipman, M. L., Rocha, A. V., Young, A. M., Kelly, R., and Dietze, M. C.: Arctic tundra fires: natural variability and responses to climate change, *13*, 369–377, <https://doi.org/10.1890/150063>, 2015.

440 Ito, A., Hajima, T., Lawrence, D. M., Brovkin, V., Delire, C., Guenet, B., Jones, C. D., Malyshev, S., Materia, S., McDermid, S. P., Peano, D., Pongratz, J., Robertson, E., Shevliakova, E., Vuichard, N., Waarlind, D., Wiltshire, A., and Ziehn, T.: Soil carbon sequestration simulated in CMIP6-LUMIP models: implications for climatic mitigation, *Environ. Res. Lett.*, *15*, 124061, <https://doi.org/10.1088/1748-9326/abc912>, 2020.

Jeong, S.-J., Bloom, A. A., Schimel, D., Sweeney, C., Parazoo, N. C., Medvigy, D., Schaepman-Strub, G., Zheng, C., Schwalm, C. R., Huntzinger, D. N., Michalak, A. M., and Miller, C. E.: Accelerating rates of Arctic carbon cycling revealed by long-term atmospheric CO₂ measurements, *4*, eaao1167, <https://doi.org/10.1126/sciadv.aao1167>, 2018.

Koven, C. D., Ringeval, B., Friedlingstein, P., Ciais, P., Cadule, P., Khvorostyanov, D., Krinner, G., and Tarnocai, C.: Permafrost carbon-climate feedbacks accelerate global warming, *PNAS*, *108*, 14769–14774, <https://doi.org/10.1073/pnas.1103910108>, 2011.

450 Lara, M. J., Nitze, I., Grosse, G., Martin, P., and McGuire, A. D.: Reduced arctic tundra productivity linked with landform and climate change interactions, *Sci Rep*, *8*, 2345, <https://doi.org/10.1038/s41598-018-20692-8>, 2018.

Lawrence, D. M., Fisher, R. A., Koven, C. D., Oleson, K. W., Swenson, S. C., Bonan, G., Collier, N., Ghimire, B., Kampenhout, L. van, Kennedy, D., Kluzek, E., Lawrence, P. J., Li, F., Li, H., Lombardozzi, D., Riley, W. J., Sacks, W. J., Shi, M., Vertenstein, M., Wieder, W. R., Xu, C., Ali, A. A., Badger, A. M., Bisht, G., Broeke, M. van den, Brunke, M. A., 455 Burns, S. P., Buzan, J., Clark, M., Craig, A., Dahlin, K., Drewniak, B., Fisher, J. B., Flanner, M., Fox, A. M., Gentine, P., Hoffman, F., Keppel-Aleks, G., Knox, R., Kumar, S., Lenaerts, J., Leung, L. R., Lipscomb, W. H., Lu, Y., Pandey, A., Pelletier, J. D., Perket, J., Randerson, J. T., Ricciuto, D. M., Sanderson, B. M., Slater, A., Subin, Z. M., Tang, J., Thomas, R. Q., Martin, M. V., and Zeng, X.: The Community Land Model Version 5: Description of New Features, Benchmarking, and Impact of Forcing Uncertainty, *11*, 4245–4287, <https://doi.org/10.1029/2018MS001583>, 2019.

460 Liang, J., Xia, J., Shi, Z., Jiang, L., Ma, S., Lu, X., Mauritz, M., Natali, S. M., Pegoraro, E., Penton, C. R., Plaza, C., Salmon, V. G., Celis, G., Cole, J. R., Konstantinidis, K. T., Tiedje, J. M., Zhou, J., Schuur, E. A. G., and Luo, Y.: Biotic responses buffer warming-induced soil organic carbon loss in Arctic tundra, *24*, 4946–4959, <https://doi.org/10.1111/gcb.14325>, 2018.

Lu, M., Zhou, X., Yang, Q., Li, H., Luo, Y., Fang, C., Chen, J., Yang, X., and Li, B.: Responses of ecosystem carbon cycle to experimental warming: a meta-analysis, *94*, 726–738, <https://doi.org/10.1890/12-0279.1>, 2013.

465 Luo, Y. and Schuur, E. A. G.: Model parameterization to represent processes at unresolved scales and changing properties of evolving systems, *26*, 1109–1117, <https://doi.org/10.1111/gcb.14939>, 2020.

Luo, Y., Ahlström, A., Allison, S. D., Batjes, N. H., Brovkin, V., Carvalhais, N., Chappell, A., Ciais, P., Davidson, E. A., Finzi, A., Georgiou, K., Guenet, B., Hararuk, O., Harden, J. W., He, Y., Hopkins, F., Jiang, L., Koven, C., Jackson, R. B., Jones, C. D., Lara, M. J., Liang, J., McGuire, A. D., Parton, W., Peng, C., Randerson, J. T., Salazar, A., Sierra, C. A., Smith, 470 M. J., Tian, H., Todd-Brown, K. E. O., Torn, M., Groenigen, K. J. van, Wang, Y. P., West, T. O., Wei, Y., Wieder, W. R., Xia, J., Xu, X., Xu, X., and Zhou, T.: Toward more realistic projections of soil carbon dynamics by Earth system models, *30*, 40–56, <https://doi.org/10.1002/2015GB005239>, 2016.

Mauritsen, T., Bader, J., Becker, T., Behrens, J., Bittner, M., Brokopf, R., Brovkin, V., Claussen, M., Crueger, T., Esch, M., Fast, I., Fiedler, S., Fläschner, D., Gayler, V., Giorgetta, M., Goll, D. S., Haak, H., Hagemann, S., Hedemann, C., 475 Hohenegger, C., Ilyina, T., Jahns, T., Jimenez-de-la-Cuesta, D., Jungclaus, J., Kleinen, T., Kloster, S., Kracher, D., Kinne, S., Kleberg, D., Lasslop, G., Kornbluh, L., Marotzke, J., Matei, D., Meraner, K., Mikolajewicz, U., Modali, K., Möbis, B., Müller, W. A., Nabel, J. E. M. S., Nam, C. C. W., Notz, D., Nyawira, S.-S., Paulsen, H., Peters, K., Pincus, R., Pohlmann,



- H., Pongratz, J., Popp, M., Raddatz, T. J., Rast, S., Redler, R., Reick, C. H., Rohrschneider, T., Schemann, V., Schmidt, H., Schnur, R., Schulzweida, U., Six, K. D., Stein, L., Stemmler, I., Stevens, B., Storch, J.-S. von, Tian, F., Voigt, A., Vrese, P.,
480 Wieners, K.-H., Wilkenskjeld, S., Winkler, A., and Roeckner, E.: Developments in the MPI-M Earth System Model version 1.2 (MPI-ESM1.2) and Its Response to Increasing CO₂, 11, 998–1038, <https://doi.org/10.1029/2018MS001400>, 2019.
- McGuire, A. D., Anderson, L. G., Christensen, T. R., Dallimore, S., Guo, L., Hayes, D. J., Heimann, M., Lorenson, T. D., Macdonald, R. W., and Roulet, N.: Sensitivity of the carbon cycle in the Arctic to climate change, 79, 523–555, <https://doi.org/10.1890/08-2025.1>, 2009.
- 485 McKane, R. B., Rastetter, E. B., Shaver, G. R., Nadelhoffer, K. J., Giblin, A. E., Laundre, J. A., and Chapin, F. S.: Climatic Effects on Tundra Carbon Storage Inferred from Experimental Data and a Model, 78, 1170–1187, [https://doi.org/10.1890/0012-9658\(1997\)078\[1170:CEOTCS\]2.0.CO;2](https://doi.org/10.1890/0012-9658(1997)078[1170:CEOTCS]2.0.CO;2), 1997.
- Mekonnen, Z. A., Riley, W. J., Randerson, J. T., Grant, R. F., and Rogers, B. M.: Expansion of high-latitude deciduous forests driven by interactions between climate warming and fire, 5, 952–958, <https://doi.org/10.1038/s41477-019-0495-8>,
490 2019.
- Myers-Smith, I. H., Kerby, J. T., Phoenix, G. K., Bjerke, J. W., Epstein, H. E., Assmann, J. J., John, C., Andreu-Hayles, L., Angers-Blondin, S., Beck, P. S. A., Berner, L. T., Bhatt, U. S., Bjorkman, A. D., Blok, D., Bryn, A., Christiansen, C. T., Cornelissen, J. H. C., Cunliffe, A. M., Elmendorf, S. C., Forbes, B. C., Goetz, S. J., Hollister, R. D., de Jong, R., Loranty, M. M., Macias-Fauria, M., Maseyk, K., Normand, S., Olofsson, J., Parker, T. C., Parmentier, F.-J. W., Post, E., Schaepman-Strub, G., Stordal, F., Sullivan, P. F., Thomas, H. J. D., Tømmervik, H., Treharne, R., Tweedie, C. E., Walker, D. A., Wilmking, M., and Wipf, S.: Complexity revealed in the greening of the Arctic, 10, 106–117, <https://doi.org/10.1038/s41558-019-0688-1>, 2020.
- Naidu, D. G. T. and Bagchi, S.: Greening of the earth does not compensate for rising soil heterotrophic respiration under climate change, n/a, <https://doi.org/10.1111/gcb.15531>, 2021.
- 500 O’Neill, B. C., Tebaldi, C., van Vuuren, D. P., Eyring, V., Friedlingstein, P., Hurtt, G., Knutti, R., Kriegler, E., Lamarque, J.-F., Lowe, J., Meehl, G. A., Moss, R., Riahi, K., and Sanderson, B. M.: The Scenario Model Intercomparison Project (ScenarioMIP) for CMIP6, 9, 3461–3482, <https://doi.org/10.5194/gmd-9-3461-2016>, 2016.
- Petrie, R., Denvil, S., Ames, S., Levvasseur, G., Fiore, S., Allen, C., Antonio, F., Berger, K., Bretonnière, P.-A., Cinquini, L., Dart, E., Dwarakanath, P., Druken, K., Evans, B., Franchistéguy, L., Gardoll, S., Gerbier, E., Greenslade, M., Hassell, D.,
505 Iwi, A., Juckes, M., Kindermann, S., Lacinski, L., Mirto, M., Nasser, A. B., Nassisi, P., Nienhouse, E., Nikonov, S., Nuzzo, A., Richards, C., Ridzwan, S., Rixen, M., Serradell, K., Snow, K., Stephens, A., Stockhouse, M., Vahlenkamp, H., and Wagner, R.: Coordinating an operational data distribution network for CMIP6 data, 1–22, <https://doi.org/10.5194/gmd-2020-153>, 2020.
- Phoenix, G. K. and Bjerke, J. W.: Arctic browning: extreme events and trends reversing arctic greening, 22, 2960–2962, <https://doi.org/10.1111/gcb.13261>, 2016.
- 510 Piao, S., Wang, X., Park, T., Chen, C., Lian, X., He, Y., Bjerke, J. W., Chen, A., Ciais, P., Tømmervik, H., Nemani, R. R., and Myneni, R. B.: Characteristics, drivers and feedbacks of global greening, 1, 14–27, <https://doi.org/10.1038/s43017-019-0001-x>, 2020.
- Qian, H., Joseph, R., and Zeng, N.: Enhanced terrestrial carbon uptake in the Northern High Latitudes in the 21st century from the Coupled Carbon Cycle Climate Model Intercomparison Project model projections, 16, 641–656, <https://doi.org/10.1111/j.1365-2486.2009.01989.x>, 2010.



- Reick, C. H., Raddatz, T., Brovkin, V., and Gayler, V.: Representation of natural and anthropogenic land cover change in MPI-ESM, 5, 459–482, <https://doi.org/10.1002/jame.20022>, 2013.
- 520 Riahi, K., van Vuuren, D. P., Kriegler, E., Edmonds, J., O'Neill, B. C., Fujimori, S., Bauer, N., Calvin, K., Dellink, R., Fricko, O., Lutz, W., Popp, A., Cuaresma, J. C., Kc, S., Leimbach, M., Jiang, L., Kram, T., Rao, S., Emmerling, J., Ebi, K., Hasegawa, T., Havlik, P., Humpenöder, F., Da Silva, L. A., Smith, S., Stehfest, E., Bosetti, V., Eom, J., Gernaat, D., Masui, T., Rogelj, J., Strefler, J., Drouet, L., Krey, V., Luderer, G., Harmsen, M., Takahashi, K., Baumstark, L., Doelman, J. C., Kainuma, M., Klimont, Z., Marangoni, G., Lotze-Campen, H., Obersteiner, M., Tabeau, A., and Tavoni, M.: The Shared Socioeconomic Pathways and their energy, land use, and greenhouse gas emissions implications: An overview, *Global Environmental Change*, 42, 153–168, <https://doi.org/10.1016/j.gloenvcha.2016.05.009>, 2017.
- 525 Richardson, A. D., Hufkens, K., Milliman, T., Aubrecht, D. M., Furze, M. E., Seyednasrollah, B., Krassovski, M. B., Latimer, J. M., Nettles, W. R., Heiderman, R. R., Warren, J. M., and Hanson, P. J.: Ecosystem warming extends vegetation activity but heightens vulnerability to cold temperatures, 560, 368–371, <https://doi.org/10.1038/s41586-018-0399-1>, 2018.
- Schuur, E. A. G. and Abbott, B.: High risk of permafrost thaw, 480, 32–33, <https://doi.org/10.1038/480032a>, 2011.
- 530 Schuur, E. A. G., McGuire, A. D., Schädel, C., Grosse, G., Harden, J. W., Hayes, D. J., Hugelius, G., Koven, C. D., Kuhry, P., Lawrence, D. M., Natali, S. M., Olefeldt, D., Romanovsky, V. E., Schaefer, K., Turetsky, M. R., Treat, C. C., and Vonk, J. E.: Climate change and the permafrost carbon feedback, 520, 171–179, <https://doi.org/10.1038/nature14338>, 2015.
- 535 Seland, Ø., Bentsen, M., Olivie, D., Toniazzo, T., Gjermundsen, A., Graff, L. S., Debernard, J. B., Gupta, A. K., He, Y.-C., Kirkevåg, A., Schwinger, J., Tjiputra, J., Aas, K. S., Bethke, I., Fan, Y., Griesfeller, J., Grini, A., Guo, C., Ilicak, M., Karset, I. H. H., Landgren, O., Liakka, J., Moseid, K. O., Nummelin, A., Spensberger, C., Tang, H., Zhang, Z., Heinze, C., Iversen, T., and Schulz, M.: Overview of the Norwegian Earth System Model (NorESM2) and key climate response of CMIP6 DECK, historical, and scenario simulations, 13, 6165–6200, <https://doi.org/10.5194/gmd-13-6165-2020>, 2020.
- Shao, P., Zeng, X., Sakaguchi, K., Monson, R. K., and Zeng, X.: Terrestrial Carbon Cycle: Climate Relations in Eight CMIP5 Earth System Models, 26, 8744–8764, <https://doi.org/10.1175/JCLI-D-12-00831.1>, 2013.
- 540 Sierra, C. A., Trumbore, S. E., Davidson, E. A., Vicca, S., and Janssens, I.: Sensitivity of decomposition rates of soil organic matter with respect to simultaneous changes in temperature and moisture, 7, 335–356, <https://doi.org/10.1002/2014MS000358>, 2015.
- Sistla, S. A., Moore, J. C., Simpson, R. T., Gough, L., Shaver, G. R., and Schimel, J. P.: Long-term warming restructures Arctic tundra without changing net soil carbon storage, 497, 615–618, <https://doi.org/10.1038/nature12129>, 2013.
- 545 Spafford, L. and MacDougall, A. H.: Validation of terrestrial biogeochemistry in CMIP6 Earth system models: a review, 14, 5863–5889, <https://doi.org/10.5194/gmd-14-5863-2021>, 2021.
- Stouffer, R. J., Eyring, V., Meehl, G. A., Bony, S., Senior, C., Stevens, B., and Taylor, K. E.: CMIP5 Scientific Gaps and Recommendations for CMIP6, *Bull. Amer. Meteor. Soc.*, 98, 95–105, <https://doi.org/10.1175/BAMS-D-15-00013.1>, 2017.
- 550 Swart, N. C., Cole, J. N. S., Kharin, V. V., Lazare, M., Scinocca, J. F., Gillett, N. P., Anstey, J., Arora, V., Christian, J. R., Hanna, S., Jiao, Y., Lee, W. G., Majaess, F., Saenko, O. A., Seiler, C., Seinen, C., Shao, A., Sigmond, M., Solheim, L., von Salzen, K., Yang, D., and Winter, B.: The Canadian Earth System Model version 5 (CanESM5.0.3), 12, 4823–4873, <https://doi.org/10.5194/gmd-12-4823-2019>, 2019.
- Tarnocai, C., Canadell, J. G., Schuur, E. a. G., Kuhry, P., Mazhitova, G., and Zimov, S.: Soil organic carbon pools in the northern circumpolar permafrost region, 23, <https://doi.org/10.1029/2008GB003327>, 2009.



- 555 Taylor, K. E., Stouffer, R. J., and Meehl, G. A.: An Overview of CMIP5 and the Experiment Design, 93, 485–498, <https://doi.org/10.1175/BAMS-D-11-00094.1>, 2012.
- Todd-Brown, K. E. O., Randerson, J. T., Post, W. M., Hoffman, F. M., Tarnocai, C., Schuur, E. a. G., and Allison, S. D.: Causes of variation in soil carbon simulations from CMIP5 Earth system models and comparison with observations, 10, 1717–1736, <https://doi.org/10.5194/bg-10-1717-2013>, 2013.
- 560 Todd-Brown, K. E. O., Randerson, J. T., Hopkins, F., Arora, V., Hajima, T., Jones, C., Shevliakova, E., Tjiputra, J., Volodin, E., Wu, T., Zhang, Q., and Allison, S. D.: Changes in soil organic carbon storage predicted by Earth system models during the 21st century, 11, 2341–2356, <https://doi.org/10.5194/bg-11-2341-2014>, 2014.
- van Vuuren, D. P., Edmonds, J., Kainuma, M., Riahi, K., Thomson, A., Hibbard, K., Hurtt, G. C., Kram, T., Krey, V., Lamarque, J.-F., Masui, T., Meinshausen, M., Nakicenovic, N., Smith, S. J., and Rose, S. K.: The representative concentration pathways: an overview, *Climatic Change*, 109, 5, <https://doi.org/10.1007/s10584-011-0148-z>, 2011.
- van Vuuren, D. P., Krieglner, E., O'Neill, B. C., Ebi, K. L., Riahi, K., Carter, T. R., Edmonds, J., Hallegatte, S., Kram, T., Mathur, R., and Winkler, H.: A new scenario framework for Climate Change Research: scenario matrix architecture, *Climatic Change*, 122, 373–386, <https://doi.org/10.1007/s10584-013-0906-1>, 2014.
- 570 Wenzel, S., Cox, P. M., Eyring, V., and Friedlingstein, P.: Projected land photosynthesis constrained by changes in the seasonal cycle of atmospheric CO₂, 538, 499–501, <https://doi.org/10.1038/nature19772>, 2016.
- Whitman, E., Parisien, M.-A., Thompson, D. K., Hall, R. J., Skakun, R. S., and Flannigan, M. D.: Variability and drivers of burn severity in the northwestern Canadian boreal forest, 9, e02128, <https://doi.org/10.1002/ecs2.2128>, 2018.
- 575 Wu, T., Lu, Y., Fang, Y., Xin, X., Li, L., Li, W., Jie, W., Zhang, J., Liu, Y., Zhang, L., Zhang, F., Zhang, Y., Wu, F., Li, J., Chu, M., Wang, Z., Shi, X., Liu, X., Wei, M., Huang, A., Zhang, Y., and Liu, X.: The Beijing Climate Center Climate System Model (BCC-CSM): the main progress from CMIP5 to CMIP6, 12, 1573–1600, <https://doi.org/10.5194/gmd-12-1573-2019>, 2019.
- Wyser, K., Kjellström, E., Koenigk, T., Martins, H., and Döscher, R.: Warmer climate projections in EC-Earth3-Veg: the role of changes in the greenhouse gas concentrations from CMIP5 to CMIP6, *Environ. Res. Lett.*, 15, 054020, <https://doi.org/10.1088/1748-9326/ab81c2>, 2020.
- 580 Yan, Y., Luo, Y., Zhou, X., and Chen, J.: Sources of variation in simulated ecosystem carbon storage capacity from the 5th Climate Model Intercomparison Project (CMIP5), 66, 22568, <https://doi.org/10.3402/tellusb.v66.22568>, 2014.
- Yue, K., Fornara, D. A., Yang, W., Peng, Y., Peng, C., Liu, Z., and Wu, F.: Influence of multiple global change drivers on terrestrial carbon storage: additive effects are common, 20, 663–672, <https://doi.org/10.1111/ele.12767>, 2017.
- 585 Zhu, Z., Piao, S., Myneni, R. B., Huang, M., Zeng, Z., Canadell, J. G., Ciais, P., Sitch, S., Friedlingstein, P., Arneeth, A., Cao, C., Cheng, L., Kato, E., Koven, C., Li, Y., Lian, X., Liu, Y., Liu, R., Mao, J., Pan, Y., Peng, S., Peñuelas, J., Poulter, B., Pugh, T. A. M., Stocker, B. D., Viovy, N., Wang, X., Wang, Y., Xiao, Z., Yang, H., Zaehle, S., and Zeng, N.: Greening of the Earth and its drivers, 6, 791–795, <https://doi.org/10.1038/nclimate3004>, 2016.
- Ziehn, T., Chamberlain, M. A., Law, R. M., Lenton, A., Bodman, R. W., Dix, M., Stevens, L., Wang, Y.-P., and Srbnovsky, J.: The Australian Earth System Model: ACCESS-ESM1.5, JSHESS, 70, 193–214, <https://doi.org/10.1071/ES19035>, 2020.
- 590 Zimov, S. A., Schuur, E. A. G., and Chapin, F. S.: Permafrost and the Global Carbon Budget, 312, 1612–1613, <https://doi.org/10.1126/science.1128908>, 2006.

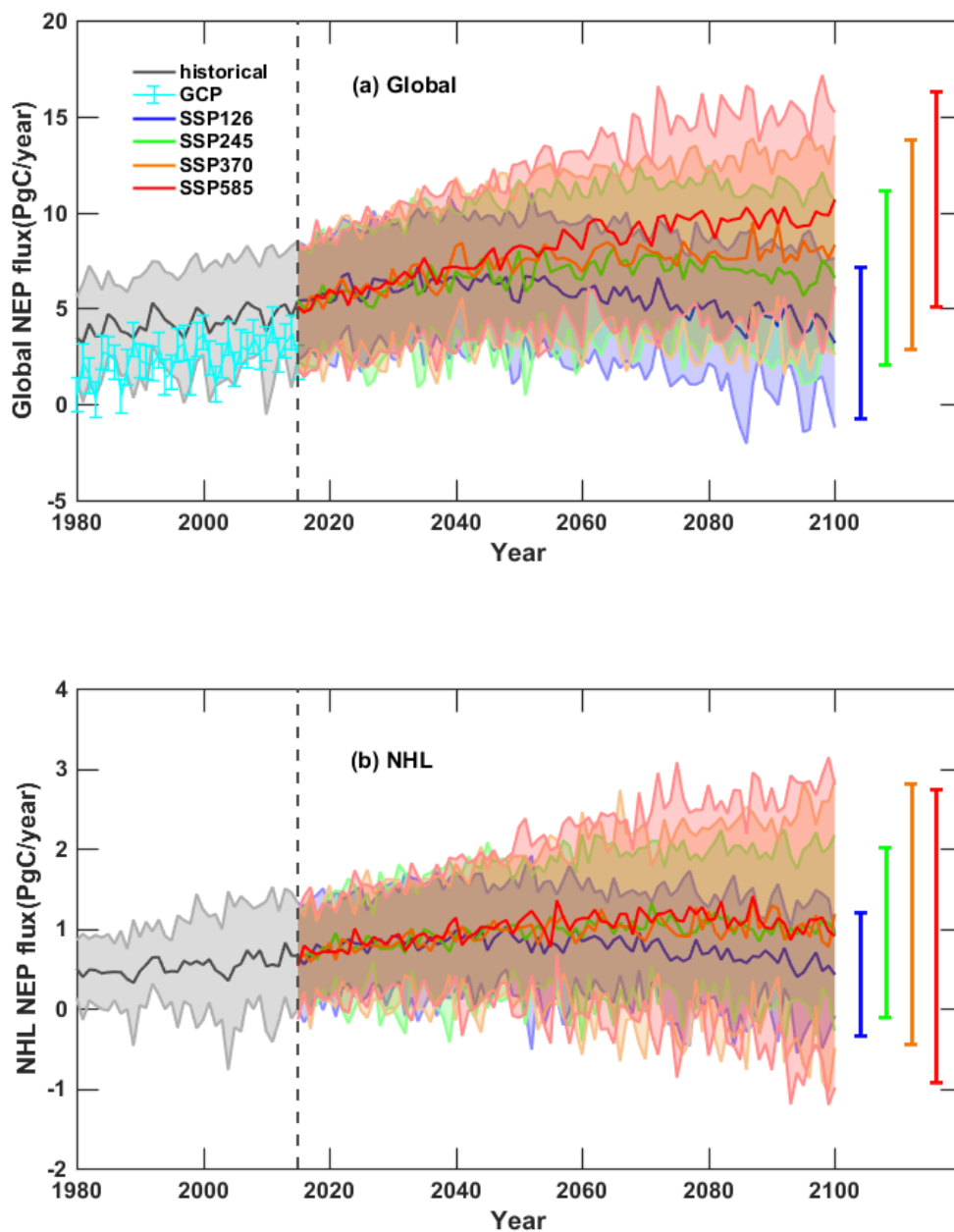
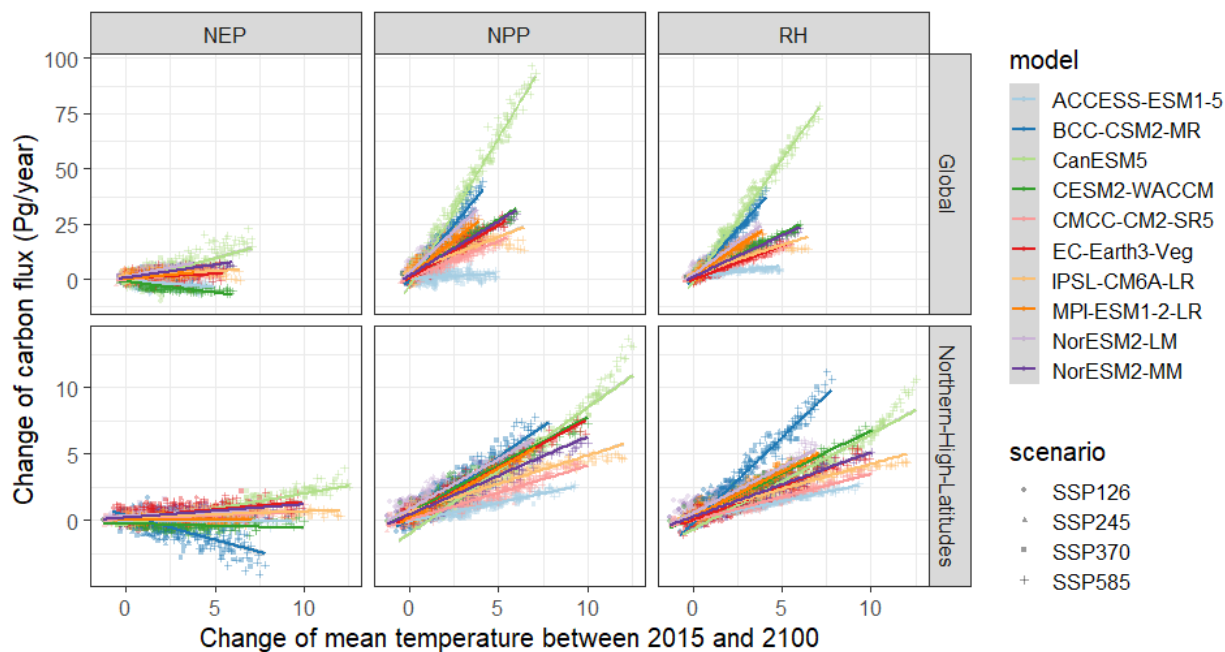
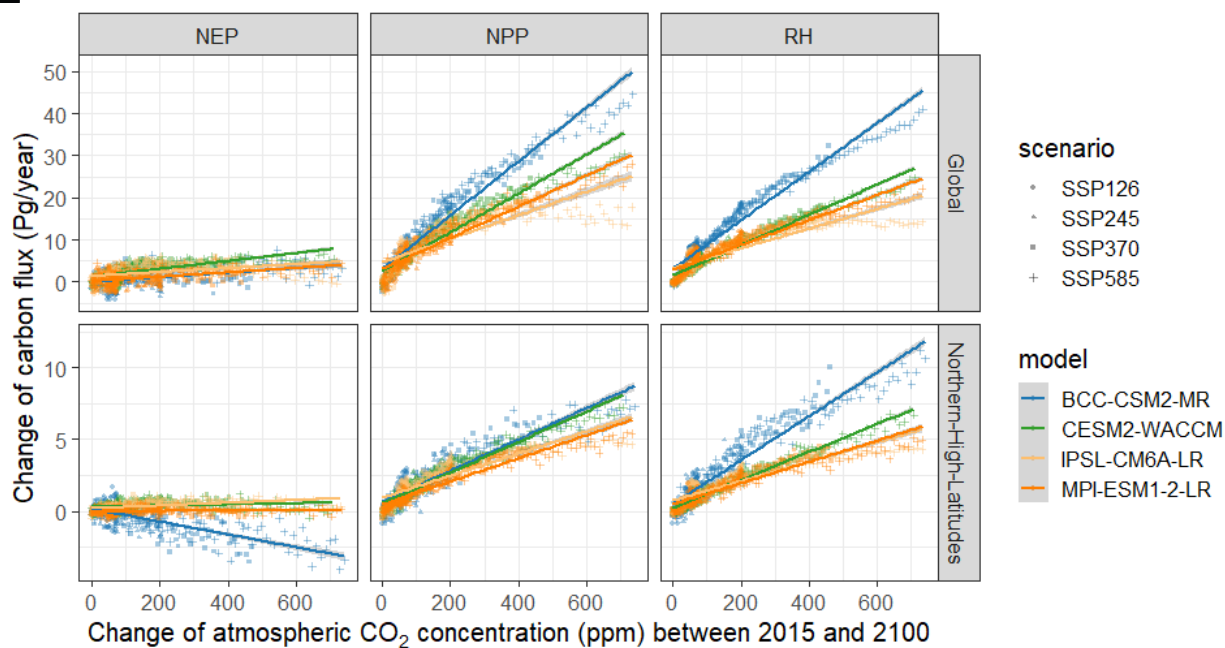


Figure 1: The annual mean NEP and SD of the ten CMIP6 models during the historical period (1980-2014) and the future period (2015 - 2100) under four global change scenarios at the global (a) and Northern High Latitude (NHL) (b) scales. The shaded area indicates the SD values across the models. Error bars at the right of the panels show the mean SD of NEPs during 2095-2100 under each of the four scenarios.



600

Figure 2: Sensitivity of carbon fluxes changes in response to the TS changes (relative to the 2015 values) at global and NHL scales for each CMIP6 model under the four future scenarios.



605 **Figure 3: Sensitivity of carbon fluxes changes in response to the CO₂ concentration changes (relative to the 2015 values) at global and NHL scales for each CMIP6 model under the four future scenarios.**

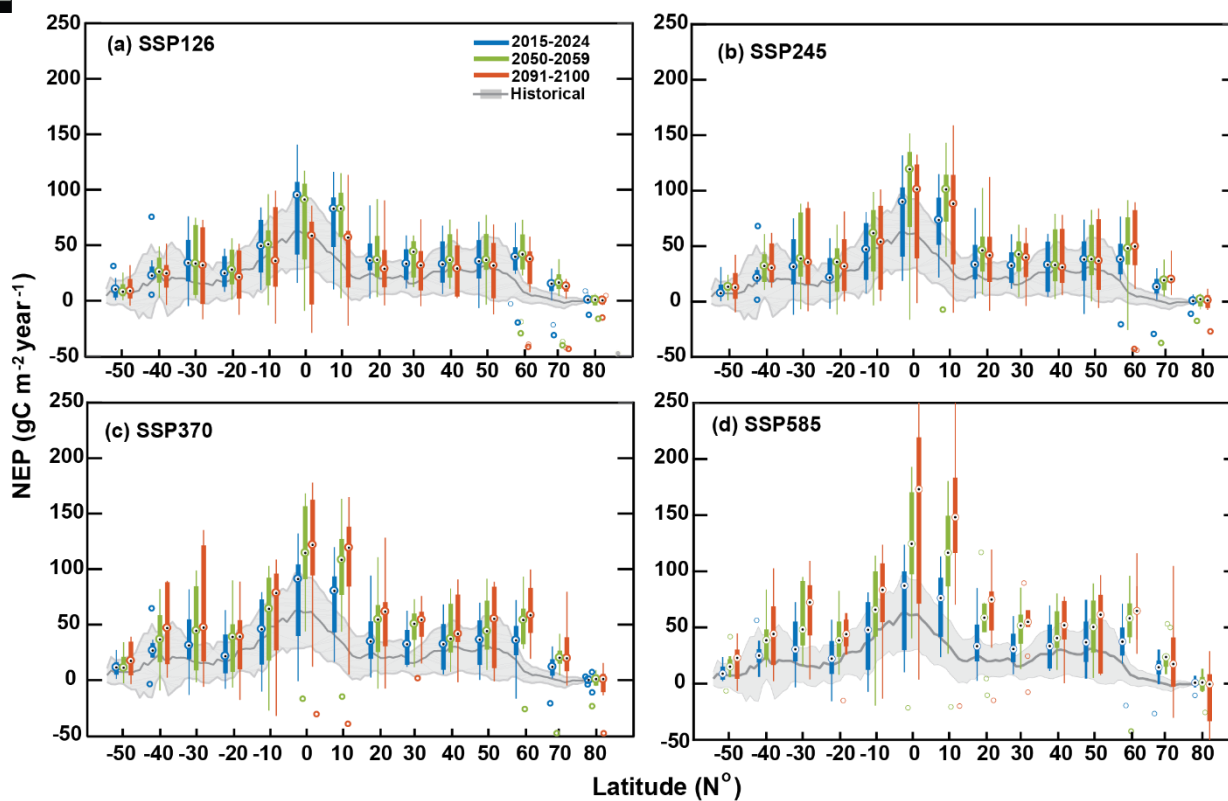


Figure 4: Latitudinal distributions of NEP in the historical period and under different future scenarios. The grey lines with bands are the historical multi-model mean and uncertainties of NEP. The boxplots are the future NEP distributed in each 10° bin between 60°S and 90°N under: (a) SSP126, (b) SSP245, (c) SSP370, (d) SSP585, during the early (2015-2024), the middle (2050-2059) and the end (2091-2100) decades of the 21st century.

610

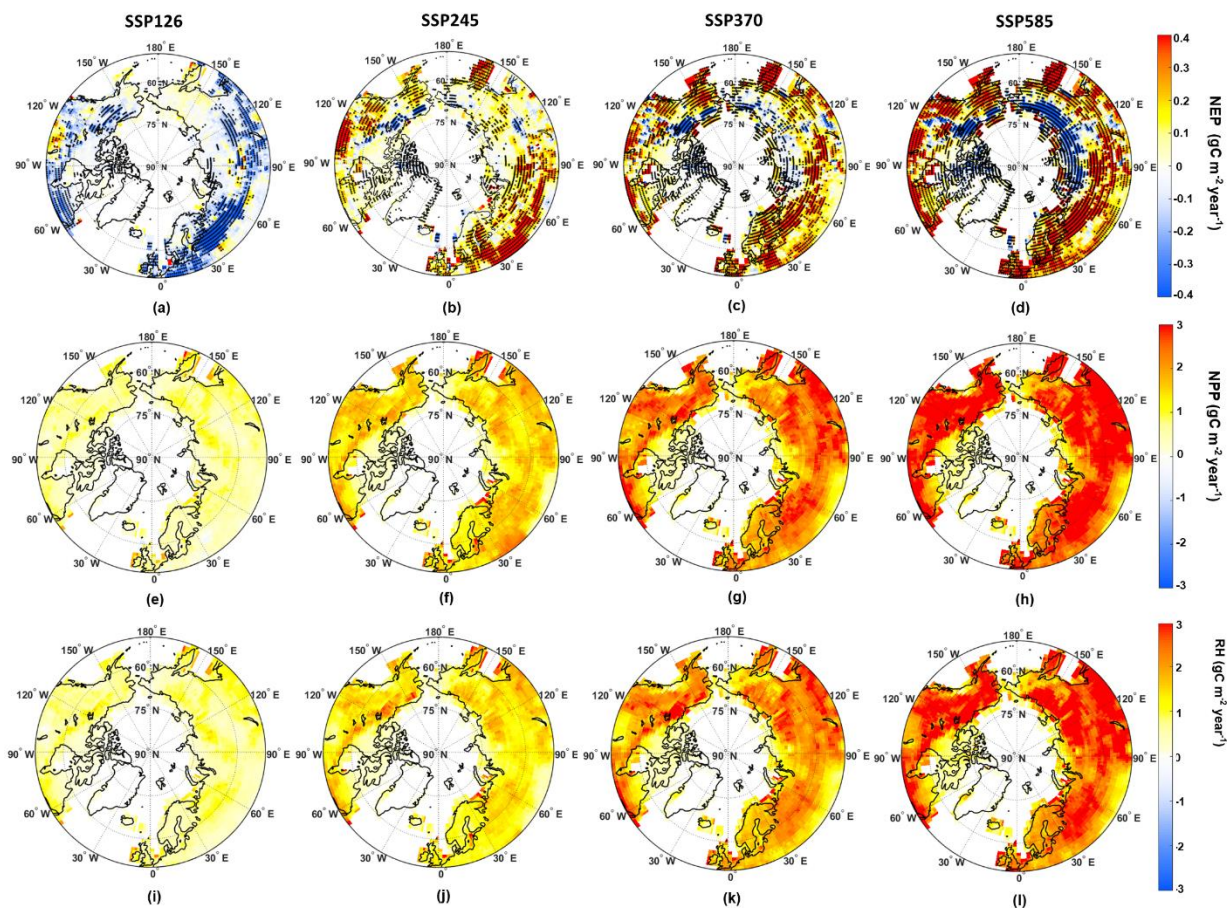
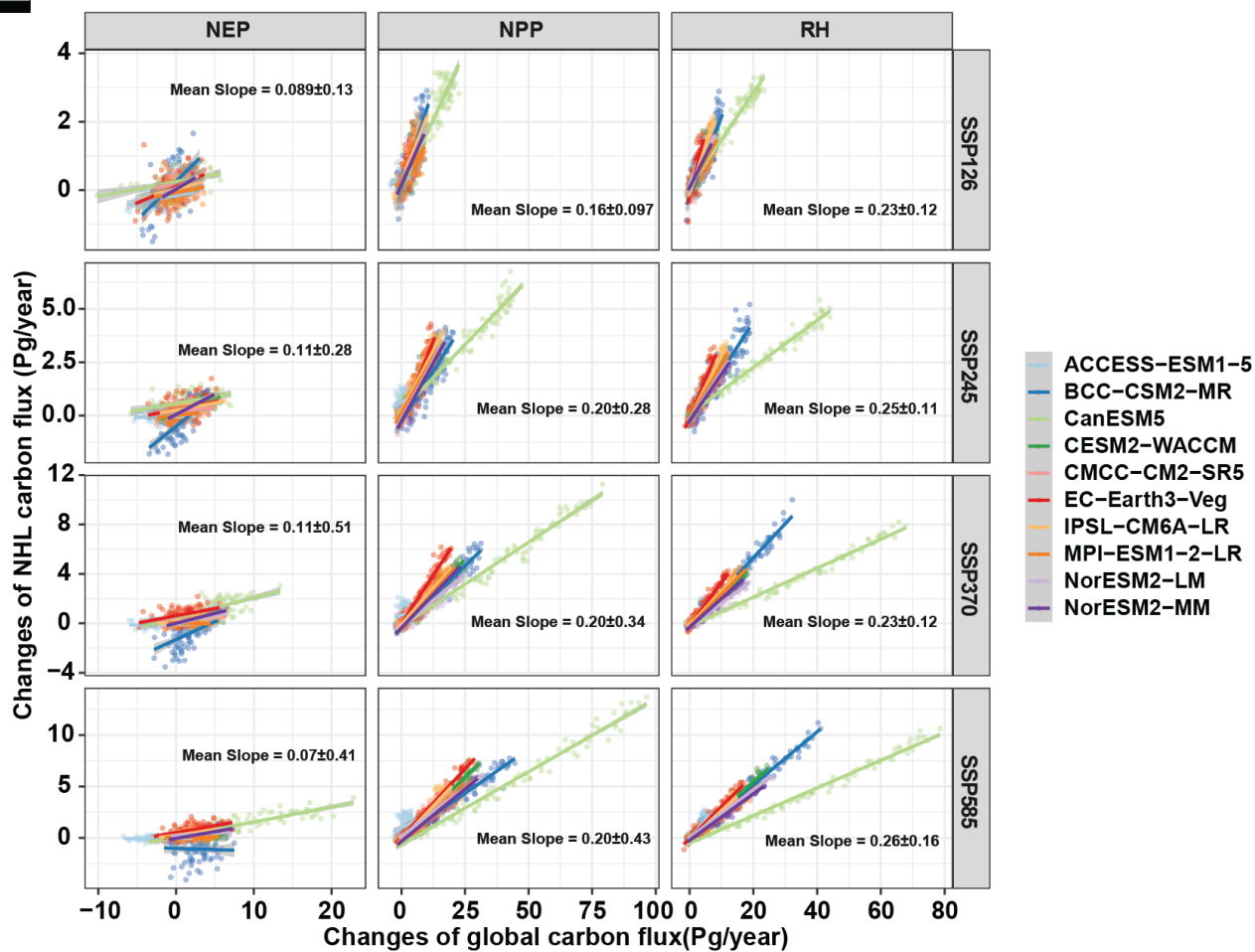


Figure 5: The spatial distributions of the trends of NHL carbon fluxes under different future scenarios. The rows of the panels are
 615 **NEP, NPP and RH from top to bottom and the columns of the panels are SSP126, SSP245, SSP370 and SSP585 from left to right.**
Unit is $g\ C\ m^{-2}\ year^{-1}$. The black dots on the NEP maps denote significance of the regression values ($p < 0.05$) when fitting the
carbon fluxes trends within each grid. Most of the model grids show significance of the regression for NPP and RH and are not
shown on the maps.

620



625

Figure 6: Simulated changes of NHL carbon fluxes relative to the changes of global carbon fluxes.

630

635



Table 1: The CMIP6 models analyzed in this study, the model land and atmosphere components, spatial resolutions and key relevant model features are listed.

Models	Component models (longitude×latitude grids)		Soil layers	N cycle	Number of Plant function types (PFTs)	Dynamic vegetation	CO ₂ fertilization effect
	Atmosphere model	Land component model					
ACCESS-ESM1-5	HadGAM2 (192×145)	CABLE2.4 (192×145)	6	Yes	13	No	Yes
BCC-CSM2-MR	BCC_AGCM3_MR (320×160)	BCC_AVIM2 (320×160)	10	Yes	15	Yes	Yes
CanESM5	CANAM5 (128×64)	CLASS3.6/CTEM1.2(128×64)	3	No	9	Yes	Yes
NorESM2-LM*	CAM-OSLO (144×96)	CLM5 (144×96)	15	Yes	15+ crop PFTs	Yes	Yes
NorESM2-MM*	CAM-OSLO (288×192)	CLM5 (288×192)	15	Yes	15+ crop PFTs	Yes	Yes
CESM2-WACCM	WACCM6 (288×192)	CLM5 (288×192)	15	Yes	15+ crop PFTs	Yes	Yes
CMCC-CM2-SR5	CAM5.3(288×192)	CLM4.5, BGC mode (288×192)	15	Yes	15+ crop PFTs	No	Yes
EC-Earth3-Veg	IFS cy36r4 (512×256)	HTESSEL (land surface scheme built in IFS) and LPJ-GUESS v4 (512×256)	2	Yes	11	Yes	Yes
IPSL-CM6A-LR	LMDZ (144×143)	ORCHIDEE v2.0, Water/Carbon/Energy mode (144×143)	11	No	15	No	Yes
MPI-ESM1-2-LR	ECHAM6.3 (192×96)	JSBACH3.20 (192×96)	5	Yes	13	Yes	Yes

* the same models but run at different spatial resolutions

640

645



Table 2: Future trends and percent changes relative to 2010-2014 for the multi-model mean NEP, NPP, RH and TS as well as their uncertainties (SD across models) of the ten CMIP6 models.

Scenarios	Trends of ensembled model mean (Tg C/year ² or °C/year ; percent change relative to 2010-2014)				Trends of model uncertainty (TgC/year ² or °C/year; percent change relative to 2010-2014)			
	SSP126	SSP245	SSP370	SSP585	SSP126	SSP245	SSP370	SSP585
Global NEP	-22.50 (20.0%)	8.93 (44.5%)	20.08 (56.8%)	44.40 (75.6%)	-2.84 (5.0%)	22.98 (17.7%)	35.03 (26.4%)	51.75 (33.5%)
Global NPP	65.72 (9.7%)	196.48 (15.9%)	294.87 (20.5%)	387.75 (24.5%)	50.10 (23.5%)	138.01 (38.7%)	219.68 (53.1%)	284.02 (63.5%)
Global RH	87.15 (9.0%)	173.39 (13.6%)	254.43 (17.6%)	318.31 (20.6%)	68.59 (16.0%)	136.77 (27.8%)	197.18 (38.0%)	228.03 (42.5%)
Global TS	0.014	0.032	0.051	0.067	0.0027	0.0033	0.0043	0.0054
NHL NEP	-2.43 (22.8%)	2.54 (53.5%)	3.08 (52.4%)	4.27 (62.9%)	-0.22 (-3.1%)	5.37 (10.4%)	11.04 (30.2%)	14.03 (45.2%)
NHL NPP	16.16 (13.9%)	41.33 (22.4%)	61.06 (26.9%)	79.32 (34.3%)	4.64 (19.3%)	8.87 (22.9%)	18.07 (41.8%)	26.87 (55.5%)
NHL RH	18.54 (13.2%)	36.27 (19.8%)	55.39 (27.8%)	72.56 (31.9%)	4.06 (9.0%)	7.76 (15.7%)	16.63 (30.2%)	23.52 (40.3%)
NHL TS	0.028	0.06	0.093	0.12	0.015	0.019	0.017	0.017